Molecular vibrations of [n]oligoacenes (n=2-5 and 10) and phonon dispersion relations of polyacene

Molecular vibrations of [*n*]oligoacenes (*n*=2–5 and 10) and phonon dispersion relations of polyacene

Yoshihiro Yamakita,[a),b)] Jin Kimura, and Koichi Ohno[a),c)]
Department of Chemistry, Graduate School of Science, Tohoku University, Aramaki, Aoba-ku, Sendai 980-8578, Japan

(Received 18 September 2006; accepted 26 December 2006; published online 12 February 2007)

As model compounds for nanosize carbon clusters, the phonon dispersion curves of polyacene are constructed based on density functional theory calculations for [*n*]oligoacenes (*n*=2–5, 10, and 15). Complete vibrational assignments are given for the observed Fourier-transform infrared and Raman spectra of [*n*]oligoacenes (*n*=2–5). Raman intensity distributions by the 1064-nm excitation are well reproduced by the polarizability-approximation calculations for naphthalene and anthracene, whereas several bands of naphthacene and pentacene at 1700–1100 cm^{-1} are calculated to be enhanced by the resonance Raman effect. It is found from vibronic calculations that the coupled a_g modes between the Kekulé deformation and joint CC stretching give rise to the Raman enhancements of the Franck–Condon type, and that the b_{3g} mode corresponding to the graphite *G* mode is enhanced by vibronic coupling between the $^1L_a(^1B_{1u})$ and $^1B_b(^1B_{2u})$ states. The phonon dispersion curves of polyacene provide a uniform foundation for understanding molecular vibrations of the oligoacenes in terms of the phase difference. The mode correlated with the defect-sensitive *D* mode of the bulk carbon networks is also found for the present one-dimensional system. © *2007 American Institute of Physics*. [DOI: 10.1063/1.2434782]

I. INTRODUCTION

Polycyclic aromatic hydrocarbons (PAH), a family of the molecules that possess carbon rings and hydrogen atoms in a plane, are common on the Earth in coal, soot, and by-products from incomplete combustion of fossil fuels.[1–3] The neutral and ionic PAHs may also be abundant in the Universe, in the form of the interstellar media emitting the unidentified infrared band.[2,4–6] The properties of PAHs have long been studied both experimentally and theoretically due to their fundamental importance in chemistry.[7,8] It is well known that some kinds of PAHs have carcinogenic activities[1,3] and that they are related with a number of photochemical phenomena.[7–9] New classes of carbon allotropes, such as fullerenes and nanotubes, may be also related with PAHs.[10,11]

As organic conductors, several PAHs play an important role in developing electronic devices[12] such as light emitting diodes, field effect transistors,[13,14] and quantum dots. For example, pentacene, of which field-effect transistors are known to exhibit very large charier mobilities,[15–18] is a well-studied system. The chemical structures of their films[19] have been studied by Raman spectroscopy,[20,21] and arranged pentacene molecules on the Au(111) (Ref. 22) or Cu(110) (Ref. 23) metal surfaces has been directly observed using scanning tunneling microscopy. On the other hand, carbon materials, notably carbon nanotubes, have also attracted many researchers[11,24] by their possibility of applications such as electronic leads and micro mechanical supports.[25–27] Graphite, including highly orientated pyrolytic graphite, is also of importance in the surface sciences. However, the intermediate-size compounds between such molecules and bulk materials are yet to be studied. The question arises, for example, as to how the systematic propensities for PAHs are connected with those of the nanosize carbon networks, and how the electron correlation plays a role in the large yet finite-size molecules. An answer would be obtained from systematic studies on the various classes of PAHs and their dehydrates (graphenes). Artificial fabrication of the carbon networks is also being developed possibly under high vacuum conditions by using, for instance, electron beam lithography[28] or a voltage on a tip of scanning tunneling microscopes.[29] Preferential syntheses of specific carbon nanotubles or size-selected clusters have become possible using laser ablation in the gas phase.[30]

The electronic properties of PAHs have been studied extensively by the electron and electronic spectroscopies.[1,31] Over the last decades, methodlogical advances have made an impact on the studies of the nanosize carbon materials. In particular, tip-enhanced methods, such as surface probe microscopy and near-field optical microscopy, have revealed the behaviors of single molecules. Vibrational excitation to a single hydrocarbon molecule leads to a primary step for surface reactions[32] and a mechanical stress on a local part of the carbon bundles give rise to the dynamics of phonon wave packets.[33] For understanding and control of chemical bondings in such systems, spectroscopic approaches may be of great help, and in particular vibrational spectroscopy would become a powerful tool in forthcoming advances. Raman studies focusing on the size-sensitive phonon bands have been performed[34,35] and the phonon dispersions of graphite

[a)]Author to whom correspondence should be addressed.
[b)]Electronic mail: yy@qpcrkk.chem.tohoku.ac.jp
[c)]Electronic mail: ohnok@qpcrkk.chem.tohoku.ac.jp

and the nanotubles have also been investigated using inelastic neutron scattering,[36] inelastic x-ray scattering,[37] and high-resolution electron energy loss spectroscopy.[38,39] Not limited within the surface sciences, mass-selected carbon clusters can also be prepared in a supersonic jet.[40]

One of the outstanding characteristics of PAHs is the strong electron correlations for conjugated π electrons. These can be monitored through vibrational frequencies and intensities, and consequently PAHs have become one of the benchmark systems for the state-of-art quantum chemical calculations. Quantum chemical calculations based on the *ab initio* molecular orbital (MO) theory and the time-dependent density functional theory (DFT) have been directed to the electronic/vibrational properties.[41–44] At the same time such properties are essentially governed by the topology of connections between carbon atoms and fundamental insights can be obtained by using semiempirical quantum chemical calculations.[45,46] The vibrational and vibronic spectra, for example, have been successfully simulated on the basis of common force fields[47,48] that are built from bond-bond polarizabilities.[49]

The simplest class of PAHs is the linear $[n]$oligoacenes, where n is the number of rings. Much attention has been paid on those with $n>8$ in recent years, motivated by the fact that the open-shell (OS) singlet *diradical* states are predicted to be the ground state.[50] For decacene, the OS diradical state was found to be 10.4 kcal mol^{-1} lower than the closed-shell (CS) singlet state, in which the singly occupied molecular orbitals are delocalized over each CCC ribbon on both sides. The diradical states may be important in the "transition" regimes of the PAH molecules toward the magnetic carbon networks. In this context polyacene is an interesting model system, although the large oligoacenes experimentally reported so far are limited up to $n=7$ of heptacene.[3,51,52] Previous quantum chemical calculations for polyacene have been focused mainly on its aromaticity and bond alternations.[53–57]

In a preliminary brief report we presented vibrational dispersion relations for polyacene based on B3LYP/4–31G calculations for those with $n<10$,[58] however, reliability was not satisfactory at that stage. Zerbi and co-workers[59] have reported similar approaches on two-dimensionally extended PAHs accounting for in-plane modes partially using their extended version[60] of Ohno's MO/8 force fields.[47,48] The vibrations of bulk graphite, especially the prominent Raman bands of the *G* (acronym for graphite) and *D* (defect) modes, have been highlighted. The origin of the Raman intensities has been successfully demonstrated utilizing internal coordinates for specific molecular motion. Thomsen and Reich have also simulated these bands under the formalism of solid-state physics and pointed out the double-resonant Raman scattering scheme.[61] However, out-of-plane modes and infrared-active modes[35] have rarely been studied, which are of importance in the finite-size systems due to possible symmetry-breaking and/or edge quantum effects. Dresselhaus and coworkers have studied the vibrational dispersions for carbon nanotubles[24,30] using empirical force fields.[62] Yumura *et al.* have reported DFT calculations for the finite-length carbon nanotubes, with respect to phase relationships for molecular vibrations.[63]

In this paper, we aim at building up rigorous foundations for all of the normal modes of the simplest one-dimensional systems. We report on the molecular vibrations of $[n]$oligoacenes ($n=2-5$ and 10) with respect to mode forms and transition intensities, and present a complete set of phonon dispersion curves for polyacene. Polyacene provides an opportunity of a cluster approach to the two-dimensional carbon networks in the $\Gamma-K$ direction, along the so-called zigzag edge.[64] Due to the large ratio of perimeter H atoms to inner C atoms, and effects from H-atom capping are also investigated. The three problems outlined above, namely, the n dependence toward the infinite system, possible diradical behaviors, and the resonance Raman effect in the correlated systems, are discussed based on experimental observations. The present work connecting the oligoacenes and polyacene can be extended in the perpendicular direction, as stacked polyacenes with finite widths.[65]

II. EXPERIMENT

Fourier-transform Raman spectra were recorded using 1064-nm excitation from a continuous wave Nd: yttrium-aluminum-garnet laser (60 mW at laser front) with a Fourier transform (FT) spectrometer (Bruker IFS66v/FRA106) which is equipped with a liquid N_2 cooled Ge detector.[66] Microcrystalline powder samples were placed in a back-scattering geometry for measurements at room temperature. Raman intensity distributions were calibrated by control experiments of standard samples. Due to the multiplex advantage of the FT spectrometer, the instrumental function for intensity was significantly flat except for the low-frequency regions, where the interference fringes from the Rayleigh-cut filter will appear. All samples were obtained as reagent grade material (>98%) from commercial sources, and were used without purification, except for pentacene which was purified by vacuum sublimation. Nevertheless a broadband persisted to overlap as a base line in the Raman spectra of pentacene and was eliminated by base line corrections. Depolarization ratios were measured when necessary after verifying that the depolarization ratios of CCl_4 were reproduced.[66]

III. CALCULATIONS

Density functional calculations were performed with the GAUSSIAN 03 program[67] on Linux-based computers and/or a supercomputer (NEC SX7) at the Research Center for Computational Science of the National Institutes of Natural Sciences. Becke's three-parameter gradient corrected exchange[68] and Lee–Yang–Parr gradient-corrected correlation functionals[69] (B3LYP) were employed throughout this work. Calculations for $n=2-5$ and those for $n=10$ and 15 were performed, respectively, on the basis of the 6-31++G(d, p) and 4-31G functions. Harmonic frequencies were calculated at optimized geometries. No scaling factor was applied to the obtained frequencies in order to avoid inconsistencies between frequency and intensity. Special care was taken to choose optional parameters for the program to avoid

TABLE I. Bond distances (Å) of [*n*]oligoacenes (*n*=2–5).[a]

	Naphthalene		Anthracene		Naphthacene		Pentacene	
	Calc	Obs[b]	Calc	Obs[c]	Calc	Obs[d]	Calc	Obs[d]
Outward CC	*1.378*	*1.378*	1.402	1.403	1.394	1.39	1.404	1.39
			1.372	*1.369*	*1.369*	*1.38*	1.390	1.38
							1.367	*1.35*
Inward CC	1.423	1.425	1.431	1.434	1.412	1.40	1.416	1.40
					1.435	1.42	1.437	1.42
Joint CC	1.435	1.426	1.446	1.441	1.453	1.46	1.458	1.45
	1.418	*1.421*	*1.428*	*1.431*	1.452	1.42	1.456	1.44
					1.432	*1.46*	*1.434*	*1.43*

[a]The terminal parameters are printed in italics. Calculated results are obtained at the B3LYP/6-31++G(*d*, *p*) level of theory.
[b]Taken from Ref. 81, which is newer than Ref. 80.
[c]Taken from Ref. 81, which is newer than Ref. 82.
[d]Reference 83.

computational errors for low-frequency modes. Relative infrared and Raman intensities were obtained by multiplying the thermally-weighted amplitude factors, $B_k(T)$, at 300 K for mode k.[70] Raman intensities also include the ν^4 frequency factors.

The B3LPY/6-31++G(*d*, *p*) level of theory provide excellent reproduction of the polarizability of benzene. Addition of the polarization functions (*d*, *p*) lead to a significant improvement in accuracy.[70] The force constants for polyacene are constructed based on those for pentadecacene (*n*=15) obtained from the B3LYP/4–31G calculations. It was verified in this work that the B3LYP/4–31G calculations give very similar results for the frequencies and infrared intensities of the oligoacenes compared the B3LYP/6-31++G(*d*, *p*) calculations. The calculated analytic force constants were folded into the force constant matrix (*F* matrix) of the repeating unit in the mass-weighted Cartesian coordinate system

$$\boldsymbol{F} = \sum_{\boldsymbol{m}=0}^{\boldsymbol{m}_{\max}} \boldsymbol{F}^{(\boldsymbol{m})} \cos m\theta, \tag{1}$$

where $F^{(0)}$ is the internal *F* matrix for the repeating unit, and $F^{(m\neq 0)}$ are those for off-diagonal *F* matrices representing interactions between the unit and the *m*th neighboring units. θ is a phase difference between adjacent units. The force constants up to those for the fifth nearest neighbors were incorporated. This approximation is justified by the fact that the calculated CC bond distances differ only by ~1% at the central position from the fifth nearest neighbor position in pentadecacene (discussed in Sec. IV B 2).

The Raman intensities at the 1064-nm excitation were calculated by two different approaches. Nonresonant Raman intensities were obtained from analytical polarizability derivatives based on the Placzek's polarizability approximation.[71,72] Preresonant Raman intensities were evaluated based on the Kramers–Heisenberg–Dirac dispersion equation[73,74] employing the formalism by Albrecht.[75] Vibronic states were obtained using the quantum chemical force fields (called MO/8 model),[47,48] where the transitions to the electronic excited states were calculated under the Pariser–Parr–Pople approximation[76,77] for self-consistent field (SCF) configuration interaction (CI) calculations, combined with the Nishimoto–Mataga approximation for the electron repulsion integrals.[78] Computational efficiency is practically crucial for treating the large correlated systems studied here. Substantial computational costs, such as those for geometry optimization, were reduced by focusing on the vertical transitions from in-plane normal modes at the ground-state geometries. As a result the vibronic properties of the $\pi-\pi^*$ excited states were successfully treated on the basis of a number of CI reference configurations. Details are given in Sec. V and the calculations for the vibronic bands in absorption spectra have been reported elsewhere.[79]

IV. RESULTS AND DISCUSSION

A. [*n*]oligoacenes (*n*=2–5)

1. Structural parameters and vibrational analyses

Table I summarizes the calculated bond distances for the oligoacenes in comparison with experimental values in the order from central to terminal ones in the D_{2h} symmetry. Agreements with the experiments seem to be satisfactory for *n*=2 (Refs. 80 and 81) and *n*=3,[81,82] which are within 0.09 Å, whereas larger deviations were obtained for *n*=5 and 6 compared with early-date experiments,[83] being 0.28 Å at maximum. The outward (inward) CC bonds on perimeters shrink (expand) upon going from the central parts to terminal ones, until they reach the maximum bond alternations at the ends. This propensity indicates the delocalization effect over the inner regions, in other words, the edge effect becomes increasingly dominant in the smaller oligoacnes. Very recently Kadantsev *et al.* have reported a similar tendency using the SVN5, PBE, and B3LYP functionals based on the 6-311++G(*d*, *p*) functions.[84] The fact that the outward or inward CC bond distances tend to increase and decrease respectively on going from *n*=2 to *n*=5 indicates the odd/even character of *n* affects the character of the π conjugation.

2. Infrared spectra

Empirical or semiempirical force fields have been reported by many researchers for naphthalene[47,85–90] and anthracene.[47,88,90,91] *Ab initio* molecular-orbital[92–96] and DFT[5,66,97] calculations have also been performed to obtain vibrational properties including transition intensities. Experi-

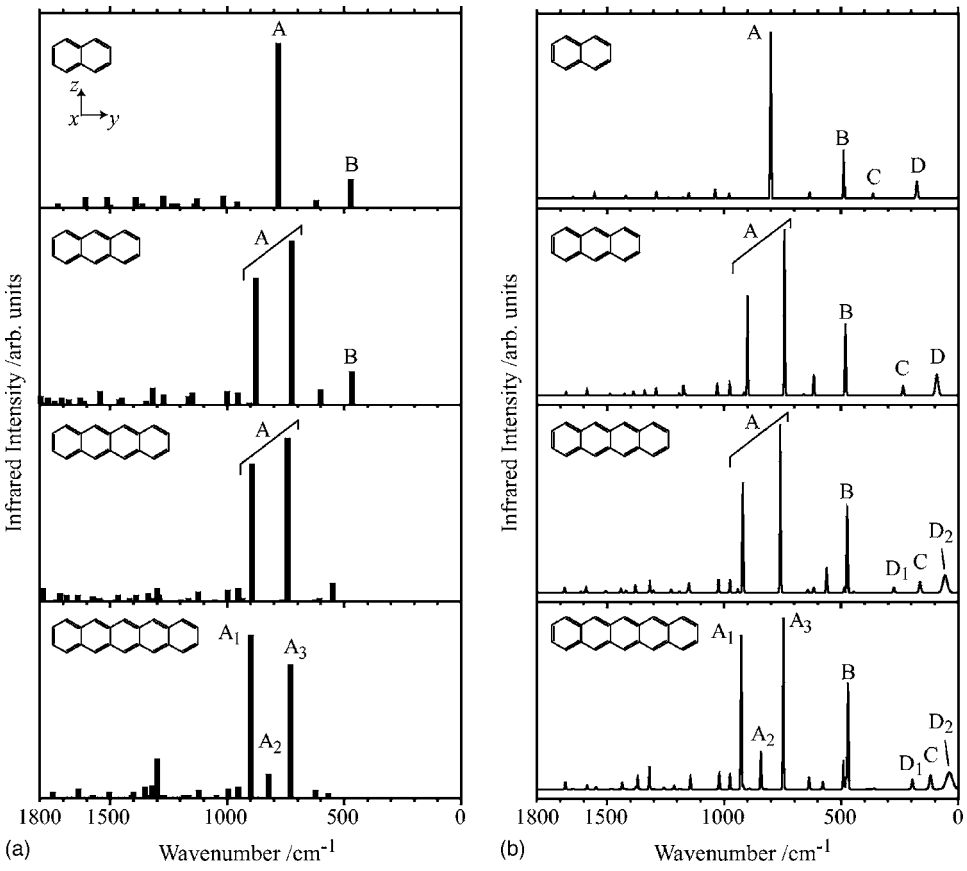

FIG. 1. Comparisons between (a) experimental (Refs. 6 and 85) and (b) calculated infrared spectra for naphthalene to pentacene. The experimental spectra do not include the far-infrared region below ~500 cm^{-1}. The calculated bands have been obtained at the B3LYP/6-31++G(d, p) level of theory, and convoluted with Gaussian bandwidths that are proportional to the thermal factors at 300 K.

mental data have been updated by modern matrix-isolation infrared spectroscopy[6] and Raman spectroscopy[89,98–103] under off-resonant[104,105] or (pre-)resonant conditions.[106–109] Vibronic bands associated with electronic transitions are of use to elucidate weak or vibrationally inactive modes, and have studied in the vapor phase[110,111] or under jet-cooled conditions.[112,113] For naphthacene and pentacene, infrared[6,114] and Raman[104,105] spectra have also been reported and they have been used as probes into crystal structures[115–118] or thin-layer morphologies[20,21] for pentacene in particular.

Figure 1 compares the calculated infrared spectra with the experimental matrix-isolation spectra reported by Hudgins and Sandford.[6,114] The experimental intensities were reproduced as stick bars in Fig. 1(a). The calculated spectra in Fig. 1(b) were convoluted with a full widths at half maximum Gaussian bandwidth of 5 cm^{-1} that is also multiplied by the thermal factor at 300 K [B_k(300)].[70] In general contribution from B_k is negligible for frequencies higher than ~400 cm^{-1} at room temperature. B_k is less than 1.2 for the region above 380 cm^{-1} and decreases monotonically toward unity for higher frequencies. The distributions of frequencies for the low-frequency modes could be broadened by their anharmonicities and/or intermolecuclar interactions, and the peak areas convoluted with B_k should be compared as transition intensities.

The most prominent bands A are commonly obtained for $n=2-5$, which are out-of-plane CH bending modes. Interestingly, they split into several bands on going to higher n. This out-of-plane CH bending modes in pentacene can be categorized in terms of their phase difference between the neighboring CH bonds, as modes A_1-A_3 depicted in Fig. 2. There are ten perimeter CH bonds apart from the edge CH bonds (see Fig. 2). In the case of mode A_1, the displacements of the H atoms at the terminal rings are almost zero, whereas they reach the maximum amplitude at the central one. Therefore,

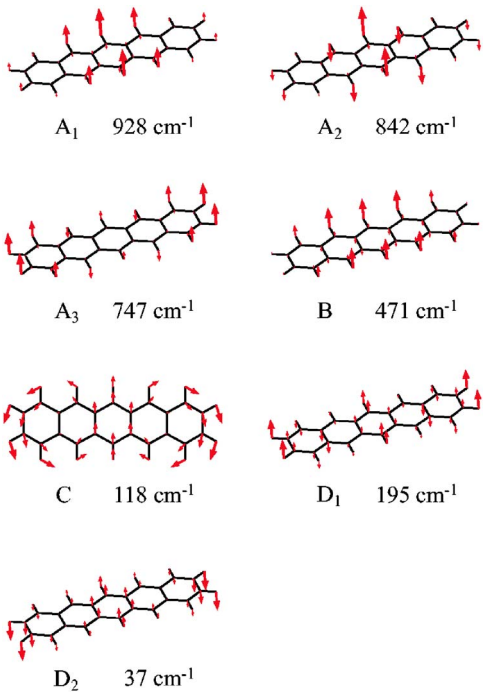

FIG. 2. Calculated normal coordinates for the strongly infrared-active modes of pentacene. Labels A_1-D_2 are the same as those in Fig. 1. The arrows are multiplied by a factor of 5.

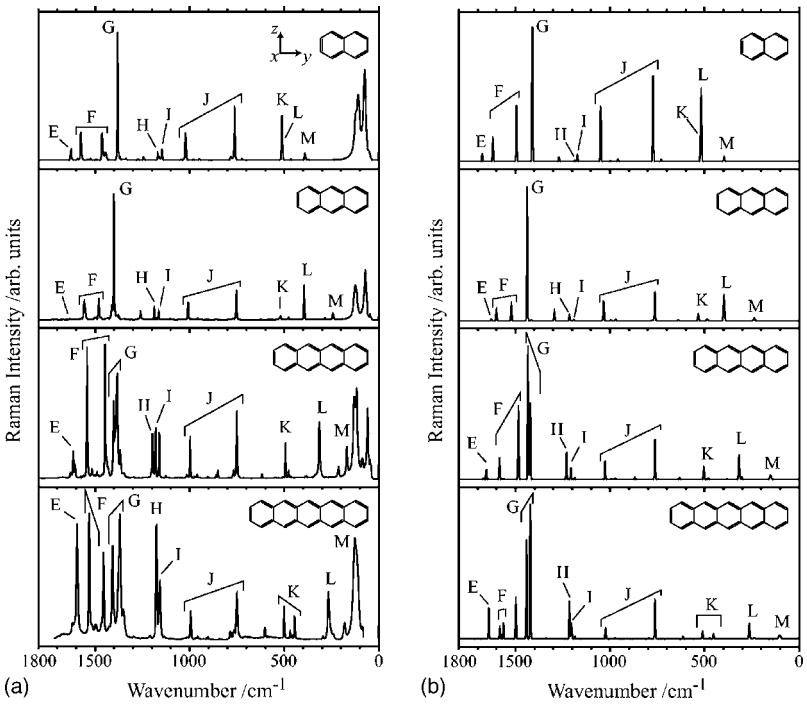

FIG. 3. Comparisons between (a) observed and (b) calculated Raman spectra for naphthalene to pentacene with the 1064-nm excitation. Nonresonant Raman spectra have been calculated at the B3LYP/6-31++G(d, p) level of theory and the calculated bands have been convoluted with Gaussian bandwidths that are proportional to the thermal factors at 300 K.

the *phase* of these displacements can be defined and is approximated to differ by π over the molecule with four translation units. Therefore, the phase difference between the neighboring CH bonds is estimated to be $\pi/4$ for mode A_1, and similarly, $\pi/2$ for mode A_2 in Fig. 2. Since the edge moieties tend to behave independently from the central parts as in mode A_3, the phase difference, θ, is just an index for categorizing the series of the normal modes. It is interesting to note that all of the displacements for the CH bonds in mode A_1 should contribute constructively to the total induced dipole moment. Such phase relations give rise to the strong infrared intensities show in Fig. 1. Conversely the out-of-phase displacements for the CH displacements in mode A_2 work destructively, and lead to relatively weak infrared intensities. Mode A_3, which is the in-phase edge motion, displays a strong infrared band. There are five ungerade modes with different phases for the ten nonedge CH bonds. One of the remaining modes appear as a weak intensity band with a destructive phase (calc 976 cm^{-1}), and the other ones belong to the infrared-inactive a_u symmetry (calc 848 and 902 cm^{-1}). These frequencies are also correlated with the phase difference.

The second strongest bands, B, are assignable to the out-of-plane ring deformation of the chair type. It may seem strange that the B bands are not present for $n=4$ and 5 in Fig. 1(a). The region below ~500 cm^{-1} is not covered by those experiments.[6,114] Frequency shifts are clearly seen for bands C and D in Fig. 1(b). These modes are connected with an entire motion over the molecule with large amplitudes (see modes C and D_2 in Fig. 2). Since the phase difference is about π between the terminal rings, it converges onto zero for larger n. When the phase difference between the neighboring units decreases to zero, modes C and D will converge to translational motion in the in-plane and out-of-plane directions, respectively. Accordingly, their frequencies undergo these marked shifts toward the zero frequency. The CH stretching modes display strong infrared intensities at ~3050 cm^{-1}.[6,114] However, these modes are found to be relatively independent of the phase relationships, and will not be discussed in this paper.

3. Raman spectra

Figure 3(a) shows the Fourier-transform Raman spectra recorded at room temperature, compared with the calculated results in Fig. 3(b). The observed broad bands in a low-frequency region below ~200 cm^{-1} are assigned to lattice vibrations.[115,119] The bandwidths reflect the crystal polymorphs and possibly the anharmonicity of the low-frequency modes. The lattice vibrations of pentacene are known to undergo frequency shifts ~10 cm^{-1} depending on crystal structures.[116–118] The Raman spectra obtained in this work have resolved the bands more clearly than those in previous studies.[104,105] Assignments for naphthalene and anthracene are in line with our previous study[66] and those for naphthacene and pentacene are obtained using the calculated Raman intensities. We first discuss the whole tendency of the Raman bands, and later describe details on assignments for naphthacene and pentacene (Sec. IV D).

Again, the systematic propensity is evident for bands $E-M$ in Figs. 3(a) and 3(b). Most bands are the totally-symmetric modes, whereas in-plane b_{3g} modes (E, I, and K) and an out-of-plane b_{1g} mode (M) are also involved. The frequencies do not change very much except for bands L and M, which shift to lower wave number upon increasing n. The vibrational patterns shown in Fig. 4 indicate that these modes are asymptotically correlated with the translational motion in the in-plane long-axis and out-of-plane directions, respectively, at the phase difference of complete zero. Bands, F, G, J, and K, show band splittings for the larger oligoacenes in Fig. 3. The phase difference of motion is responsible for this. The strongest bands, G, arise from combination modes of the

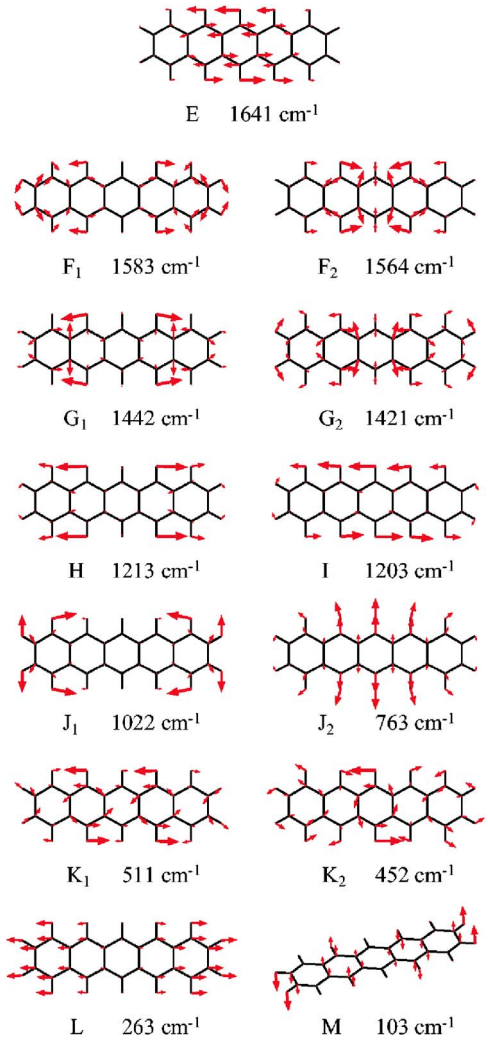

FIG. 4. (Color online) Calculated normal coordinates for the strongly Raman-active modes of pentacene. Labels $E-M$ are the same as those in Fig. 3. The arrows are multiplied by a factor of 5.

so-called Kekulé vibrations. The Kekulé vibration is localized at the terminal rings in mode G_1 depicted in Fig. 4, whereas the next-central ones in mode G_2. The fact that these strongest band intensities are taken over by the F bands of joint CC stretching is connected with the excited states involved in these Raman processes. Agreement/disagreement with the nonresonant Raman intensity calculations can be assessed in the following manner.

Tables II and III present the assignments by listing numerical values for the frequencies and Raman intensities. The Raman-scattering activity is an intrinsic value of a molecule which does not include the effects from the ν^4 factor. The assignments are obtained straightforwardly for almost all of the observed bands. Those for weaker bands are reinforced by use of the calculated intensities, and also by the systematic propensities mentioned earlier. The calculated frequencies are found to be systematically higher than the experimental values, but no scaling factor was used since scaled force constants are related with different normal coordinates and wave functions. The reproducibility of the intensity calculations can be discussed more quantitatively by evaluating the rood-mean-square (rms), σ, for the logarithms of the intensity ratios $I_k^{\mathrm{calc}}/I_k^{\mathrm{obs}}$,[66]

TABLE II. Vibrational frequencies (cm^{-1}) and Raman intensities for naphthalene (except CH stretches).

	Calc[a]				Obs	
Sym	Freq	Activ[b]	Int[c]	Mode	Freq	Int[c]
a_g	1620	0.341	0.18	*F*	1577	0.29
	1495	0.711	0.40	*F*	1464	0.34
	1411	1.689	1.00	*G*	1382	1.00
	1186	0.012	0.01	*H*	1169	0.08
	1049	0.571	0.41	*J*	1022	0.31
	773	0.792	0.65	*J*	764	0.48
	519	0.430	0.42	*K*	514	0.33
b_{3g}	1676	0.101	0.05	*E*	1628	0.12
	1493	0.039	0.02		1444	0.13
	1269	0.048	0.03		1244	0.03
	1172	0.076	0.05	*I*	1147	0.10
	947	0.000	0.00		937	0.00
	517	0.231	0.23	*L*	509	0.12
b_{1g}	958	0.023	0.02		949	0.02
	730	0.016	0.01		725	0.02
	397	0.037	0.04	*M*	393	0.08
b_{2g}	999	0.006	0.01		980	0.02
	897	0.002	0.00		*869*[d]	0.00
	781	0.000	0.00		–	–
	481	0.002	0.00		466	0.02

[a]Unscaled results calculated at the B3LYP/6-31++G(d, p) level of theory.
[b]The Raman-scattering activities $(45\alpha'^2+7\beta'^2)/\tilde{\nu}$ are given in the unit of $(4\pi\varepsilon_0)^2 a_0^4/(\mathrm{u\ cm}^{-1})$, where a_0 is the Bohr radius and u is the atomic mass unit. The ν^4 wavelength dependence is not involved.
[c]Intensities relative to the strongest bands. The wavelength dependence and the temperature factors are included. Accordance factor $\alpha=0.426$.
[d]Very weak.

$$\sigma = \sqrt{\frac{1}{n}\sum_{i=1}^{n}\left[\log_a\left(\frac{I_k^{\mathrm{calc}}}{I_k^{\mathrm{obs}}}\right)-b\right]^2}, \tag{2}$$

$$b = \frac{1}{n}\sum_{i=1}^{n}\log_a\left(\frac{I_i^{\mathrm{calc}}}{I_i^{\mathrm{obs}}}\right), \tag{3}$$

where I_k^{calc} and I_k^{obs} are, respectively, the kth calculated and observed intensities on an arbitrary linear scale. If we evaluate the rms without the logarithm, serious disagreement(s), e.g., a factor of 10, will predominantly determine the results. The logarithmic deviation (σ) is converted to the linear scale to yield the deviation factor (δ) and the accordance factor (α), as

$$\delta = a^{\sigma}, \tag{4}$$

$$\alpha = 1/\delta. \tag{5}$$

These indicate that the average deviation of the calculated intensities from the observed intensities is given by the factor δ (or $1/\delta$). δ takes a value in the range of $[1, \infty]$ (corresponding to complete agreement or disagreement, respectively), and α takes values in the range $[0, 1]$ (again corresponding to complete disagreement or agreement). The evaluation of α employs only the strong bands for which relative intensities are greater than a threshold value 0.05. Otherwise the ratios of very weak intensities will introduce significant numerical errors to the results.

TABLE III. Vibrational frequencies (cm^{-1}) and Raman intensities for anthracene (except CH stretches).

	Calc[a]				Obs	
Sym	Freq	Activ	Int	Mode	Freq	Int
a_g	1600	0.798	0.09	*F*	1557	0.30
	1522	1.149	0.13	*F*	1481	0.17
	1438	8.473	1.00	*G*	1402	1.00
	1294	0.582	0.07	*H*	1260	0.09
	1191	0.064	0.01		1164	0.07
	1034	1.035	0.15	*J*	1008	0.13
	764	1.283	0.22	*J*	753	0.21
	640	0.026	0.01		623	0.01
	398	0.911	0.21	*L*	396	0.24
b_{3g}	1674	0.005	0.00	*E*	1634	0.02
	1627	0.088	0.01		1577	0.01
	1416	0.031	0.00		1377	0.04
	1298	0.000	0.00		1275	0.00
	1213	0.340	0.05	*I*	1187	0.09
	1127	0.001	0.00		1103	0.01
	926	0.002	0.00		915	0.01
	533	0.286	0.06	*K*	520	0.04
	394	0.159	0.04		391[b]	0.02
b_{1g}	970	0.062	0.01		956	0.02
	772	0.017	0.00		772[c]	0.02
	486	0.060	0.01		479	0.03
	237	0.084	0.03	*M*	243	0.08
b_{2g}	995	0.019	0.00		977	0.00
	915	0.000	0.00		901	0.00
	844	0.000	0.00		–	–
	779	0.008	0.00		772[c]	0.02
	589	0.001	0.00		579	0.00
	270	0.000	0.00		286	0.02

[a]Unscaled results calculated at the B3LYP/6-31++G(*d*, *p*) level of theory. Details on definitions are given in the footnotes of Table II. Accordance factor α=0.506.
[b]Shoulder.
[c]Overlapped.

The thermal factors, $B_k(T)$,[70] which were not taken into account in our previous study,[66] have been incorporated in this work. Their contributions are not negligible (>10%) for bands below 400 cm^{-1}, like bands *L* and *M* for *n*=4 and 5 in Fig. 3. The resulting accordance factors are α=0.426 and 0.506 for *n*=2 and 3, respectively. These values are comparable or better than those for the previous BLYP/6-31G(*d*) calculations,[66] which are α=0.478 (*n*=2) and 0.180 (*n*=3). However, these are worse than the combined calculations with the MO/8 normal coordinates and the BLYP/6-31G(*d*) polarizability derivatives,[66] where α=0.676 (*n*=2) and 0.606 (*n*=3).

The results for naphthacene and pentacene are given in Tables IV and V, respectively. The accordance factors for intensity are estimated to be α=0.454 (*n*=4) and 0.316 (*n*=5). These values obviously indicate poor agreements. These disagreements are also evident in Fig. 3 for bands *E*–*I* and *M*. The high-frequency bands labeled *E*, *F*, *H*, and *I* markedly gain their intensities for *n*=4 and 5 in the observed spectra. In particular, the *F* bands which are assigned to the joint CC stretching mode (Fig. 4) are stronger than bands *G* of the Kekulé mode. Such a tendency has not been observed for pyrene and perylene at the 1064-nm excitation, where the accordance factor were found to be α=0.606 and 0.508, respectively.[66]

TABLE IV. Vibrational frequencies (cm^{-1}) and Raman intensities for naphthacene (except CH stretches).

	Calc[a]				Obs	
Sym	Freq	Activ	Int	Mode	Freq	Int
a_g	1584	2.189	0.16	*F*	1543	0.80
	1563	0.076	0.01		1517	0.05
	1484	6.971	0.55	*F*	1448[b]	1.09
	1434	12.375	1.00	*G*	1404	0.59
	1422	7.059	0.57	*G*	1384	1.00
	1230	2.265	0.20	*H*	1197	0.32
	1187	0.134	0.01		1160	0.23
	1026	1.439	0.14	*I*	997	0.22
	869	0.153	0.02		851[b]	0.04
	763	2.683	0.31	*J*	752	0.44
	632	0.112	0.01		618	0.02
	317	1.367	0.24	*L*	315	0.58
b_{3g}	1667	0.165	0.01		1629	0.04
	1654	1.049	0.08	*E*	1617	0.17
	1483	0.071	0.01		1448[b]	1.09
	1360	0.013	0.00		1348	0.02
	1293	0.000	0.00		1271	0.00
	1207	0.986	0.09	*I*	1180	0.25
	1152	0.007	0.00		1126	0.01
	907	0.003	0.00		904	0.01
	786	0.001	0.00		773	0.01
	504	0.752	0.09	*K*	494	0.16
	304	0.133	0.02		304	0.01
b_{1g}	973	0.104	0.01		960	0.02
	865	0.000	0.00		851[b]	0.04
	746	0.028	0.00		718	0.01
	480	0.087	0.01		478	0.04
	384	0.021	0.00		385[c]	0.02
	151	0.208	0.06	*M*[d]	170	0.23
b_{2g}	994	0.032	0.00		970	0.01
	918	0.002	0.00		910	0.00
	854	0.001	0.00		–	–
	773	0.018	0.00		769	0.03
	730	0.000	0.00		711	0.00
	521	0.001	0.00		508	0.00
	192	0.001	0.00		216	0.08

[a]Unscaled results calculated at the B3LYP/6-31++G(*d*, *p*) level of theory. Details on definitions are given in the footnotes of Table II. Accordance factor α=0.454.
[b]Overlapped.
[c]Doublet.
[d]Coupled with lattice vibrations.

4. Resonance Raman effect

One possibility for those disagreements, except those for bands*M*, is the resonance Raman effect. The obvious discrepancies for *n*=4 and 5 are in contrast to the case of *n*=2 and 3 (Fig. 3). We note that the S_0–S_1 absorption energies of naphthacene (2.71 eV, extrapolated to gas phase)[41,120] and pentacene (2.23 eV)[41,120] are much smaller than those of PAHs of similar sizes, pyrene (3.33 eV, methanol solution)[121] and perylene (2.85 eV, tetrahydrofuran solution).[122] Figure 5 illustrates the excitation energies for the oligoacenes studied for the purpose of comparisons with the excitation energy of

TABLE V. Vibrational frequencies (cm^{-1}) and Raman intensities for pentacene (except CH stretches).

	Calc[a]				Obs	
Sym	Freq	Activ	Int	Mode	Freq	Int
a_g	1583	2.667	0.09	*F*	1532	0.46
	1564	3.449	0.12	*F*	1498	0.04
	1498	8.430	0.30		1456	0.30
	1442	20.349	0.74	*G*	1408	0.89
	1421	27.280	1.00	*G*	1370[b]	1.00
	1338	0.175	0.01		1295	0.01
	1213	6.889	0.28	*H*	1176	0.45
	1186	0.419	0.02		1135	0.01
	1022	2.007	0.09	*J*	995	0.11
	797	0.156	0.01		786	0.02
	763	5.716	0.30	*J*	751	0.21
	645	0.001	0.00		–	–
	615	0.335	0.02		603	0.03
	263	1.823	0.16	*L*	266	0.15
b_{3g}	1676	0.032	0.00		1619	0.07
	1641	7.146	0.23	*E*	1596	0.67
	1596	0.056	0.00		1569	0.00
	1421	0.125	0.01		1370[b]	1.00
	1316	0.001	0.00		1252[c]	0.00
	1296	0.001	0.00		1242[c]	0.00
	1245	0.051	0.00		1210	0.01
	1203	2.796	0.11	*I*	1157	0.33
	1158	0.007	0.00		–	–
	933	0.013	0.00		909	0.00
	723	0.003	0.00		–	–
	511	1.013	0.06	*K*	501	0.09
	452	0.677	0.04	*K*	446	0.06
	237	0.128	0.01		240	0.02
b_{1g}	975	0.148	0.01		957	0.01
	892	0.002	0.00		–	–
	754	0.037	0.00		–	–
	481	0.000	0.00		469	0.01
	473	0.132	0.01		460	0.01
	296	0.038	0.00		295	0.01
	103	0.421	0.07	*M*[d]	127	–
b_{2g}	994	0.042	0.00		968	0.00
	919	0.012	0.00		902	0.01
	874	0.002	0.00		841	0.00
	839	0.001	0.00		–	–
	771	0.031	0.00		766	0.02
	748	0.000	0.00		–	–
	553	0.001	0.00		–	–
	348	0.000	0.00		–	–
	149	0.004	0.00		182[d]	–

[a]Unscaled results calculated at the B3LYP/6-31++G(*d*, *p*) level of theory. Details on definitions are given in the footnotes of Table II. Accordance factor α=0.316.
[b]Overlapped.
[c]Tentatively assigned to a very weak band.
[d]Coupled with lattice vibrations (Ref. 89).

1064 nm (1.17 eV). For naphthalene and anthracene, Ohta and Ito have demonstrated the resonance Raman effect using various excitation wavelengths in a range 351.1 nm (3.53 eV)–632.8 nm (1.96 eV).[106,107] Those bands corresponding to $E-I$ clearly gain their intensities on going from 632.8 to 457.9 nm (2.71 eV) excitations.[107]

Figure 6 shows the calculated transition intensities for the vibronic bands associated with the S_0-S_1 electronic transitions for naphthacene and pentacene. It is widely accepted that the vibronic bands of the Franck–Condon and vibronic-coupling types have parallel relationships with the *A* and *B* terms for the resonance Raman effect.[107,123,124] Figure 6 clearly shows that modes $F(a_g)$ and $H(a_g)$ have the Franck–Condon activities upon the S_0-S_1 transition of the ^1L_a type. Modes $E(b_{3g})$ are calculated to be enhanced through the vibronic coupling between the ^1L_a and ^1B_b transitions, which is in line with the cases of n=2 and 3.[106,107] Interestingly, the bands *F* and *H* which involve the joint CC stretching (see Fig. 4) are much enhanced in observation of Fig. 3(a). This fact is related with the structural changes associated with the $\pi-\pi^*$ excitation from highest occupied molecular orbital (HOMO) to lowest unoccupied molecular orbital (LUMO). Indeed, the HOMOs (b_{2g}) and LUMOs (b_{3u}) of all of the oligoacenes studied have the antibonding and bonding characters with respect to the joint CC bonds, respectively, leading to the Franck–Condon changes localized there. However, the fact that modes F_2 does not show a strong Raman en-

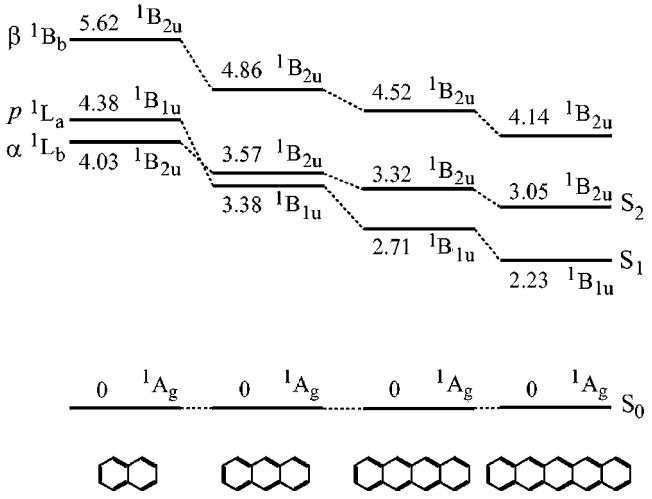

FIG. 5. Electronically excited states of oligoacenes. Numbers are energy differences in electron volts taken from Refs. 41 and 91.

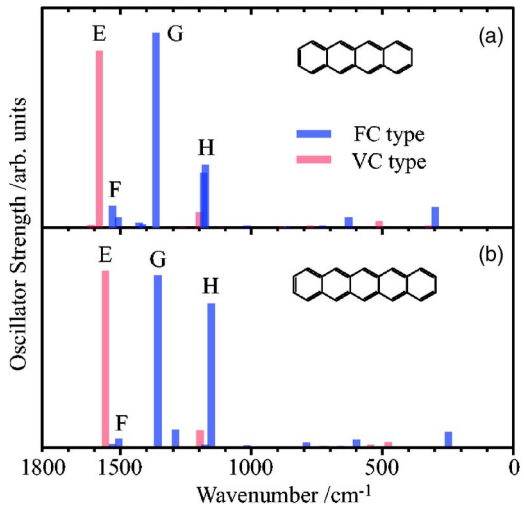

FIG. 6. (Color online) Calculated oscillator strengths of (a) naphthacene and (b) pentacene for the $S_1 \leftarrow S_0$ electronic transitions of the Franck–Condon type (in blue) and the vibronic-coupling ones (in red). Scales between the two types are arbitrary.

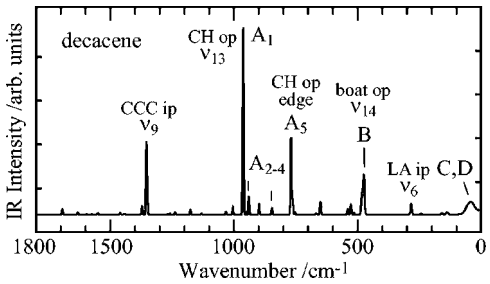

FIG. 7. Infrared spectra of decacene in the closed-shell singlet state calculated at the B3LYP/4–31G level of theory. The labels of assignments are the same as in Fig. 8.

hancement compared to F_1 indicates the importance of the structural changes at the edge rings and/or the outward CC bonds in the excited states involved. Bands $E(b_{3g})$ are observed four times stronger for $n=5$ than for $n=4$ in Fig. 3(a) (see also Tables IV and V). These Raman enhancements have been ascribed to the vibronic coupling between the $^1L_a(^1B_{1u})$ and $^1B_b(^1B_{1u})$ states. On the other hand, the nonresonant Raman intensities calculated for this mode are three times stronger for $n=5$ than for $n=4$ in Fig. 3(b), which is parallel with the observed intensities.

It may seem strange that the $G(a_g)$ bands, which display the strong Franck–Condon activities, do not become strong for $n=4$ and 5 in Fig. 3(a) relative to the Franck–Condon active bands $F(a_g)$ and $H(a_g)$. This phenomenon can be explained by accounting for the higher states and their vibronic couplings. In the Raman enhancements of the vibronic coupling type, two excited electronic states are involved [see Eq. (14)], and the $^1B_b(^1B_{1u})$ state which possesses the very large absorption coefficients[41,120] is likely to play a key role. Indeed, bands F and G are calculated to have the vibronic-coupling intensities for $n=4$ and 5 between the $^1B_b(^1B_{2u})$ and $^1L_b(^1B_{2u})$ states, where the orbital-forbidden ^1L_b state $(b_{3u} \leftarrow b_{1g})$ couples with the orbital-allowed ^1B_b state $(a_u \leftarrow b_{2g})$ through the displacements of these a_g modes. Moreover these vibronic-coupling intensities are calculated to interfere constructively with those of the Franck–Condon type for the $S_0-S_1(^1L_a)$ transition in the case of bands F, whereas destructively for bands G.

B. Decacene ($n=10$)

1. Infrared activity

Figure 7 presents the calculated infrared spectra of decacene in the CS singlet state. Bands A_1-A_5 in Fig. 7, which arise from out-of-plane CH bending mode, change their infrared intensities drastically depending upon the phase difference. In other words the intensities reflect the balances of vibrational motion. When the induced dipole moments work additively at all of the CH bonds, as depicted in Fig. 2, the total dipole moment leads to the most prominent band, A_1. On increasing the phase difference from π to 3π, 5π, and 7π over the ten pairs of the perimeter CH bonds in nine units of lattice constants, the intensity for this out-of-plane mode decreases as those of bands A_2, A_3, and A_4 in Fig. 7. The edge CH bonds vibrate independently and give rise to an isolated out-of-plane mode of band A_5. In the case of even harmonics, 2π, 4π, …, induced dipole moments are balanced out by the opposite vibrational displacements at the right and left sides. Bands C and D, in-plane and out-of-plane transversal motion, respectively, have almost converged to the zero frequency. The bands at ~ 280 cm^{-1} are assigned to the in-plane ring mode which forms a longitudinal motion in direction of the long molecular axis.

TABLE VI. Calculated bond distances (Å) for decacene and pentadecacene in the closed-shell singlet states.[a]

	Decacene	Pentadecacene
Outward CC	1.402	1.403
	1.399	1.403
	1.394	1.402
	1.385	1.401
	1.364	1.398
		1.394
		1.385
		1.364
Inward CC	1.404	1.404
	1.407	1.405
	1.411	1.406
	1.418	1.408
	1.437	1.411
		1.419
		1.437
Joint CC	1.467	1.469
	1.467	1.469
	1.466	1.469
	1.463	1.468
	1.459	1.466
	1.434	1.463
		1.460
		1.434

[a]Calculated at the B3LYP/4–31G level of theory. The terminal parameters are printed in italics.

The OS singlet state is calculated to have an energy 8.6 kcal mol^{-1} lower than the CS state at the B3LYP/4–31G level. Although the result is in line with the previous results at the BPW91/6-31G(d) and BLYP/6-31G(d) level calculations,[50,56] the calculated wave functions show large spin contamination, $\langle S^2 \rangle = 1.41$. Similarly the OS state of pentadecacene ($n=15$) is calculated to be 20.0 kcal mol^{-1} lower than the CS state with very large spin contamination, $\langle S^2 \rangle = 2.36$. Although nonsinglet states are anticipated to arise as the ground state anyway on going from small PAHs to any bulk state, the reliability of the calculated OS wave functions are yet to be confirmed.[56] Therefore, we will not discuss the results further in the present paper.

2. Bond alternations

Table VI shows the degree of bond alternations for decacene and pentadecacene based on the B3LYP/4–31G calculations. For both molecules, the shrinking/expanding behavior is clearly obtained at the perimeter CC bonds toward the maximum alternations at the ends. The almost identical distances between the outward/inward CC bonds indicate their convergence to those in the infinitely long system. The C_{2h} symmetry type of alternations, where CC double bonds face to each other in a trans form with respect to the inver-

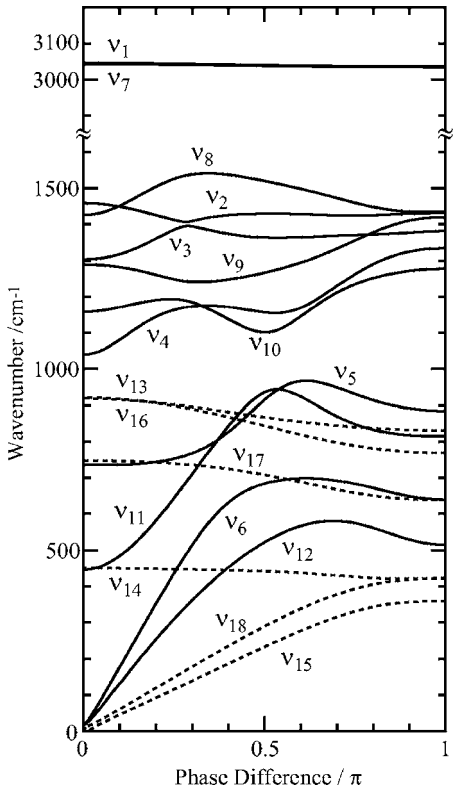

FIG. 8. Calculated phonon dispersion relations for polyacene in the closed-shell singlet state. Broken lines represent out-of-plane modes.

sion center,[54] have not been obtained in this work. The CC bond distances of real systems, graphite and benzene for example, are 1.42 and 1.397 Å, respectively. Therefore, these perimeter CC bonds are close to those in benzene, and the joint CC bonds are much longer than these sp^2 CC bonds. These structural parameters are connected with the local aromaticity, on which many studies have been reported so far based on various indexes such as the bond order.[53–57]

C. Polyacene

1. Dispersion relations

The vibrational modes of the oligoacenes have been well described in terms of the phase difference, θ, of vibrational displacements. Figure 8 shows vibrational dispersion relations for all modes of polyacene in the closed-shell singlet state, which was obtained from the force constants of pentadecacene. Symmetry species are degraded to a factor group for the repeating unit. The symmetry properties that are invariant by the definition of a unit cell include the mirror plane and the C_2 axis pointing to the long axis. Hence, it is reasonable to define the unit cell as the vertical linkage of HCCCCH in the C_{2v} point group. The degree of vibrational freedom is thus represented as $\Gamma^{ip}=6a_1+6b_2$ and $\Gamma^{op}=3a_2+3b_1$, resulting in eighteen modes or *branches* in total, where ip and op denote in-plane and out-of-plane, respectively. No mode mixing takes place between the in-plane and out-of-plane branches and neither between the symmetric and antisymmetric ones with respect to the mirror plane. Within the same species, the no crossing rule will operate quantum mechanically when they come close to each other. It is noted

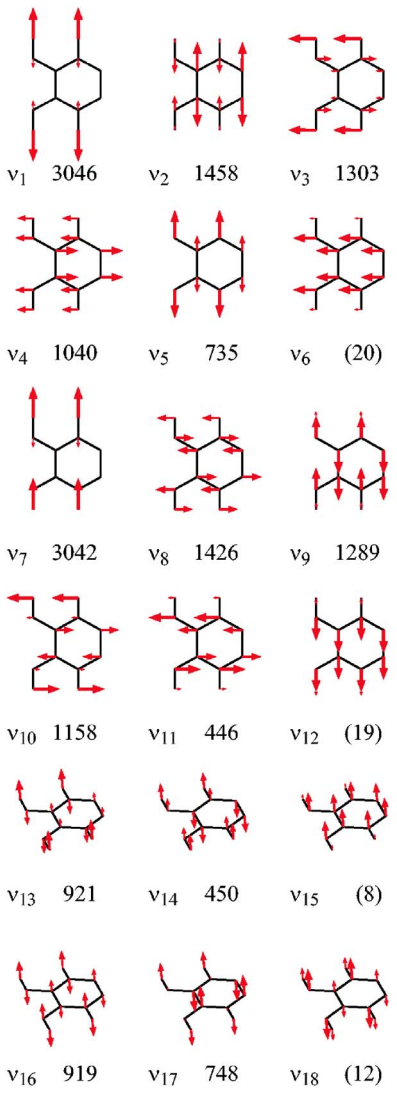

FIG. 9. (Color online) Calculated normal coordinates for polyacene in the closed-shell state at the phase difference $\theta=0$ rad. Two units are depicted for viewing ring motion. The arrows are multiplied by a factor of 2.5. Numbers are the calculated frequencies in cm^{-1}, and those for the acoustic modes are given in parentheses.

that the infrared or Raman activities of the oligoacenes are not determined solely in relation with the above factor group. The inversion properties of gerade/ungerade depend on the phase difference.

The in-plane modes are comprised of the $\nu_1-\nu_6$ modes in the a_1 symmetry and the $\nu_7-\nu_{12}$ modes in the b_2 symmetry. Figure 9 depicts the vibrational mode patterns for polyacene at the zero phase difference. For easy viewing of ring motion, two repeating units are included. An approximate relevance between the finite and infinite systems is $A:\nu_{13}$, $B:\nu_{14}$, $C:\nu_{12}$, $D:\nu_{15}$, $E:\nu_8$, $F:\nu_2$, $G:\nu_3$, $H:\nu_4$, $I:\nu_{10}$, $J:\nu_5$, $K:\nu_{11}$, $L:\nu_6$,.and $M:\nu_{15}$ Apart from the CH stretching modes ν_1 and ν_7, the other branches ν_9, ν_{16}, ν_{17}, and ν_{18} are less sensitive to the infrared and Raman spectroscopies and have no counterparts. The same branch can lead to both infrared and Raman bands at different θ, as bands D and M. The most interesting behavior would be the mixing between the CC stretching and CCC bending as a function of the phase difference. It is most clearly seen be-

tween the ν_2 and ν_3 modes at the avoided crossing. At the zone center, these modes are best described by the CCC deformation and CC stretching respectively (Fig. 9), whereas will be converted to the joint CC stretching and the Kekulé vibrations, as modes *F* and *G* in Fig. 3. These modes and mode ν_4 give rise to the resonance Raman effect of the Franck–Condon type (bands *F*, *G*, and *H*). Another important mode is ν_8, which is connected with the vibronic coupling between the $^1L_a(^1B_{1u})$ and $^1B_b(^1B_{2u})$ states (bands *E*). The observed Raman spectra in Fig. 3(a) are almost dominated by the totally-symmetric modes arising from combinations of $\nu_1-\nu_6$. The out-of-plane modes are calculated to be below $\sim 900\ \mathrm{cm}^{-1}$, comprising $\nu_{13}-\nu_{15}$ in the a_2 symmetry and $\nu_{16}-\nu_{18}$ in the b_1 symmetry. The ν_{13} and ν_{14} modes display the most prominent infrared bands. The out-of-plane modes $\nu_{16}-\nu_{18}$ in the a_2 symmetry tend to become infrared/Raman inactive modes belonging to the a_u symmetry.

It is interesting to remark the modes which converge to the origin. As can be seen in Fig. 9, the ν_6 branch is the longitudinal acoustic mode, in the *y* direction, whereas ν_{12} and ν_{15} are the transversal ones in the *z* and *x* directions, respectively. The ν_{18} mode is connected with a torsion around the long molecular axis at $\theta \neq 0$ and converges to a rotation on the *y* axis at $\theta=0$. As mentioned in Secs. IV A and IV B, these modes (bands *C*, *D*, *L* and *M*) can be regarded as an indicator for the length of oligoacenes. The rotations on the *x* and *z* axes are automatically removed from the dispersion relations since they cannot be represented by vibrations with finite amplitudes under the repeating condition in the *y* direction. The above four acoustic modes, ν_6, ν_{12}, ν_{15}, and ν_{18}, have not converged completely to the zero frequency, as the frequencies in parentheses in Fig. 9. These values represent the incompleteness of the present approximation for the force constants. First of all, perhaps it is highly difficult to obtain the zero frequency in the Cartesian-coordinate space. In general, large-amplitude vibrations would tend to be sensitive to long-range small force constants. Second, the employed interacting force constants between the repeating units are not those for the real infinite system. They represent for those units located at outer positions from the central ones in pentadecacene. We have seen that the fifth nearest neighbor still has a small bond alternation, 1.394 Å vs 1.411 Å (1.2%) for the CS state in Table VI.

2. Relations with carbon materials

The results obtained for hypothetical polyacene would show relevance to the real systems. It is well known that the phonon dispersion relation makes it possible to estimate physical properties. The slopes of the acoustic modes are connected with the velocities of the propagating waves, and the force constants of the accordionlike vibrations (the ν_6 branch) will provide the elasticity (the Young's modulus).[125] Above all, the fused rings studied here correspond to the $\Gamma-K$ dispersions for the hexagonal lattice of graphite,[37–39,62] and one can attempt to find correlations with the six branches of graphite. When we disregard the CH modes (ν_1, ν_4, ν_7, ν_{10}, ν_{13}, and ν_{17}) as independent vibrations from the CC ones, there are 12 branches left (Fig. 9). The unit cell of graphite is defined to be a CC bond. In the analogy with the present case, the positions equivalent to the graphite CC bond are located at the joint CC bonds and the CH bonds. The antiphase relations for the two CC and two CH bonds, respectively, correspond to the dispersions at the *K* and *M* points in the inverse lattice space since their phase differences are $\pi/2$. Modes ν_3, ν_5, ν_9, ν_{11}, ν_{14}, and ν_{18} always show antiphase relations between the bonds at the CC and CH positions in polyacene, and therefore represent dispersions at the *M* position. It follows that changes in the phase relations in the *y* direction with keeping this phase difference in the *z* direction lead to dispersions in $M-K$ directions.[37,62] The branches representing the in-phase motion for all of the four bonds at $\theta=0$, i.e., ν_2, ν_6, ν_8, ν_{12}, ν_{15}, and ν_{16}, are correlated with the six branches of bulk graphite in the $\Gamma-K$ directions[62] (SH, LA, LO, SH, ZO, and ZA, respectively, in the notation in Ref. 38). Resemblances are recognized for the optical branches among these modes, ν_2, ν_8, and ν_{17}, with those of bulk graphite, except that the ν_2 and ν_8 branches are not crossed near the position of $\theta=\pi$ in Fig. 8. In other words, these vibrations involving the CC bonds are not perturbed very much by the small mass of H atoms in these regions. However, the acoustic branches, ν_6, ν_{12}, and ν_{15}, indicate much more floppy and elastic properties for polyacene.

We could also discuss correlations for the resonance Raman bands for the two-dimensional lattices and one-dimensional polyacene. Two strong Raman bands known as the *G* and *D* bands give rise to the strong resonance Raman effect. The *G* mode of bulk is barely correlated with the ν_8 branch in Fig. 9 as mode *E* in Fig. 4 (or Fig. 3). In the case of graphite, where the *G* mode at the Γ point belongs to the totally symmetric group, the resonance Raman effect would be described by the Franck–Condon type or the vibronic-coupling type between the excited states with the same symmetry. In contrast, the defect-sensitive *D* mode of bulk is known to display vibrational patterns like the breathing mode between the *K* and *M* points.[59] The mode of polyacene closest to the modes would be derived from the ν_3 branch in Fig. 9, like mode *G* in Fig. 4, since the dispersion of the ν_3 modes is located in a range $1350-1300\ \mathrm{cm}^{-1}$ in Fig. 8. The fact that modes G_1 and G_2 shows ring motion essentially for every other ring supports the previous models for the Raman intensity of the bulk *D* mode, where the *D* mode gains its activity from as vibrations in the multifold lattice structures.[59] Frequency dependences of the *D* mode[34,126,127] in the range $1310-1380\ \mathrm{cm}^{-1}$ match those for the ν_3 branch. The polarization of the S_0-S_1 absorption in the oligoacenes is perpendicular to the long axis, whereas that of the *D* band is located between the in-plane long and short axes, or between the *M* and *K* points.[61,126,127] The present results for hydrogen-capped graphene would present comparative information by extending the conjugation to the other in-plane direction.[65] For instance, the (n, n) single-wall carbon nanotubes with the armchair edges[24] can be investigated in comparison with them. Moreover, the phonon dispersions of polyacethylene is found to be well correlated as a subgroup of polyacene.[128] This indicates significant independence for

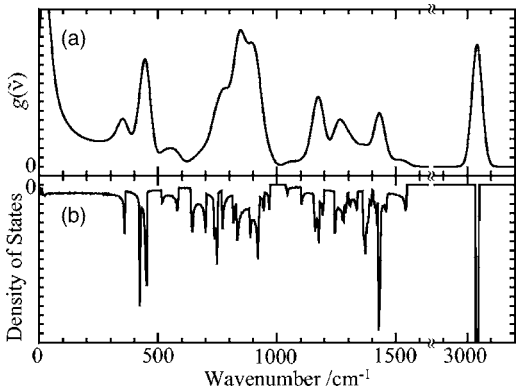

FIG. 10. Densities of vibrational states weighted by the squares of vibrational amplitudes for the hydrogen atoms, $g(\tilde{\nu})$, and densities of vibrational states for polyacene in the closed-shell singlet state. The $g(\tilde{\nu})$ spectra have been convoluted with a full width at half maximum Gaussian bandwidth of 50 cm^{-1}.

the modes of the side CCC ribbons of polyacene from the perturbations of mode mixing via the joint CC bonds, and also the validity of electron mobility in the long acene systems.

3. Density of states in phonon dispersions

Figure 10 shows the density of vibrational states for polyacene in the closed-shell singlet states. The density of states determines the cross sections for wave vector-sensitive experiments including the inelastic neutron scattering, the inelastic x-ray scattering, and the electron energy loss spectroscopy. They are sensitive to group motion in bulk materials. In particular, the cross sections for the incoherent inelastic neutron scattering are known to be determined by the Debye–Waller factor to which the amplitudes of H atoms have dominant contributions.[129] The predicted cross sections $g(\tilde{\nu})$ shown in Fig. 10 displays strong bands at ~880 cm^{-1}. In this region the CH out-of-plane bending modes, ν_{13} and ν_{16}, have large densities of states since these modes are less dispersive over the phase difference. In the case of polyacene the ratio of H atoms to C atoms are significant compared to the carbon materials, and the cross-sections will be determined the phonon motion involving the perimeters. These cross sections $g(\tilde{\nu})$ are usually observed as convoluted bands as in Fig. 10(a). On the other hand, the densities of states shown in Fig. 10(b) are composed of sharp peaks. Those obtained at 400–500 cm^{-1} and ~1420 cm^{-1} arise from the out-of-plane ν_{14} branch and the ν_2 branches of skeletal mode. In general, the optical branches show slopes of nearly zero at $\theta=0$ and $\theta=\pi$ and give rise to sharp peaks at highest and lowest frequency positions of the branches which are connected by smooth curves in Fig. 10.

D. Spectral assignments

The vibrational assignments for the Raman-active modes of naphthacene and pentacene are given in Tables IV and V, respectively. To our best knowledge, the complete vibrational assignments including gerade modes, particularly those based on DFT calculations, have not been reported for these molecules.[5] The calculated frequencies and intensities are found to be sufficiently good to allow unique assignments for almost all of the Raman bands, however, the following may be worth being mentioned.

1. Naphthacene

(1) Band M observed at 170 cm^{-1}, which is calculated to be much lower at 151 cm^{-1} (−11%), is likely to be coupled with lattice vibrations (see Table IV and Fig. 3). This tendency is also obtained for bands M of $n=2$ (−1%) and $n=3$ (−3%), as listed in Tables II and III. The next candidate at 131 cm^{-1} in Fig. 3(a) displays too strong an intensity for this out-of-plane mode. Filippini and Gramaccioli have also assigned the 170 cm^{-1} band to the coupled intramolecular mode, and low-frequency bands at 131, 118, 62, and 48 cm^{-1} to lattice modes, respectively.[115]

(2) Strong bands at 1607, 1395, and 1368 cm^{-1} remain unassigned in Table IV. Possible origins for these bands include the Davydov splitting and combinations/overtones enhanced by the Fermi resonance. The observed strong intensity of the 1160 cm^{-1} band in Fig. 3 is not reproduced by the calculation. This discrepancy is most likely to due to the enhancement by the Fermi resonance. In the vicinity of band G, relatively strong bands were observed as shoulders at 1395 and 1368 cm^{-1}. Band E is also accompanied by small shoulder bands in Fig. 3(a). Such unassigned bands were carefully deconvoluted from the fundamental modes, for which intensities are given in Table IV.

(3) Mode F is observed to be stronger than band G in contrast to the large Franck–Condon activity for band G in Fig. 6(a). This fact is due to the interference with the resonance Raman effect of the vibronic coupling type (discussed in Sec. IV A 4).

2. Pentacene

(1) It is not straightforward to find an appropriate observed band for the out-of-plane M mode calculated at 103 cm^{-1} (Table V and Fig. 3). Valle *et al.* have reported lattice dynamics calculations, where this mode is calculated to couple with lattice modes significantly.[118] The abnormally strong band at 127 cm^{-1} in Fig. 3(a) is assigned to the M mode, which is calculated to be significantly lower (−10%). Mixing between the intra- and intermolecular vibrations tends to give rise to remarkable upward shifts for the fundamental bands. The prominent band observed at 182 cm^{-1} in Fig. 3(a) is also calculated to be lower, as the b_{2g} mode at 149 cm^{-1} (Table V). These frequency discrepancies increasingly become evident from $n=4$ onwards, due to the frequency convergence toward the zero frequency for the acoustic modes of the large oligoacenes. It is noted that the shape of band L is very asymmetric despite its less coupling with lattice vibrations.[118]

(2) The mode forms of bands F and G are characterized by the joint CC stretching and the Kekulé vibration, respectively (Fig. 4). Nonetheless the lower one of the F bands in Fig. 3(a) does not display a strong Raman intensity. This is in contrast to the case of naphthacene, where two strong bands are observed as modes F. The odd or even number of the rings could be correlated with these different behaviors,

since the inversion symmetry of vibrational modes and/or excited electronic states play a key role for these Raman activities.

V. COMPUTATIONAL DETAILS

Cross sections for the resonance Raman scattering are given by the Kramers–Heisenberg–Dirac dispersion equation.[73,74] For a process from the initial state $|m\rangle=|g\rangle|u\rangle$ to the final state $|n\rangle=|g\rangle|v\rangle$ via the intermediate state $|r\rangle=|e\rangle|w\rangle$, the total intensity of scattered light $I_{m\to n}$ in the 4π solid angle is expressed by

$$I_{m\to n} \propto (\omega_0+\omega_{mn})^4 \sum_{i,j} |(\alpha_{ij})_{m\to n}|^2 I_0, \tag{6}$$

$$(\alpha_{ij})_{m\to n} = \frac{1}{\hbar} \sum_{r\neq m,n} \left[\frac{\langle m|\mu_j|r\rangle\langle r|\mu_i|n\rangle}{\omega_{rm}-\omega_0-i\gamma_r} + \frac{\langle m|\mu_i|r\rangle\langle r|\mu_j|n\rangle}{\omega_{rn}+\omega_0+i\gamma_r} \right]. \tag{7}$$

where I_0 is the energy flux of the excitation light with the angular velocity ω_0, a_{ij} is the (i, j) component of the polarizability tensor with respect to the space-fixed frame (XYZ), γ_r is the damping constant for the transitions involving state r, and $\omega_{mn}=\omega_m-\omega_n$. The total wave functions $|n\rangle$, $|m\rangle$, and $|r\rangle$ are approximated as the products of the electronic wave functions $|r\rangle$, $|e\rangle$ and the vibrational wave functions $|u\rangle$, $|v\rangle$, and $|w\rangle$ for nonrotating molecules. In Eq. (6) the operators are those for two dipole moments in direction i or j following the Placzek's polarizability approximation.[71,72]

The variations of electronic transition moment $(\mathbf{M})_{ge}=\langle g|\boldsymbol{\mu}|e\rangle$ with respect to the dimensionless normal coordinates $\{q_k\}$ is expressed in the form of the Herzberg–Teller expansion

$$\boldsymbol{M}_{ge} = \boldsymbol{M}^0_{ge} + \sum_k \left(\frac{\partial \boldsymbol{M}_{ge}}{\partial q_k}\right)_0 q_k + \cdots, \tag{8}$$

$$\left(\frac{\partial \boldsymbol{M}_{ge}}{\partial q_k}\right)_0 = \sum_{s\neq e} \boldsymbol{M}^0_{gs} \frac{\left[\left\langle e\left|\frac{\partial H}{\partial q_k}\right|s\right\rangle\right]_0}{E^0_e - E^0_s}. \tag{9}$$

Hence, the resonance Raman intensities can be described by incorporating the normal-coordinate displacements,[75]

$$(\boldsymbol{\alpha})_{m\to n} = \boldsymbol{A}+\boldsymbol{B}+\boldsymbol{C}, \tag{10}$$

$$A_{ij} = \frac{1}{\hbar}\sum_{e,w} (M_i)^0_{ge}(M_j)^0_{ge}\left(\frac{1}{\omega_{ew,gu}-\omega_0} + \frac{1}{\omega_{ew,gv}+\omega_0}\right)\langle u|w\rangle\langle w|v\rangle, \tag{11}$$

$$B_{ij} = \frac{1}{\hbar}\sum_{e,w} (M_i)^0_{ge}\frac{1}{\omega_{ew,gu}-\omega_0}\sum_k \left[\frac{\partial (M_j)_{ge}}{\partial q_k}\right]_0 \langle u|w\rangle\langle w|q_k|v\rangle + \frac{1}{\hbar}\sum_{e,w} (M_j)^0_{ge}\frac{1}{\omega_{ew,gu}-\omega_0}\sum_k \left[\frac{\partial (M_i)_{ge}}{\partial q_k}\right]_0 \langle u|q_k|w\rangle\langle w|v\rangle, \tag{12}$$

where i, j are vibrational states in the ground states and w includes vibronic states in the excited states. The term C is the nonresonant counterpart of the B term. Summing up the intermediate vibrational states on assumption that the vibrational energies are negligible, $\omega_{ew,\,gu}=\omega_e$ for all w and u, yields[75,123,124]

$$A'_{ij} = \frac{2}{\hbar^2}\sum_e \frac{(\omega_e^2+\omega_0^2)}{(\omega_e^2-\omega_0^2)^2}(M_i)^0_{ge}(M_j)^0_{ge} \times \sum_k \left[\left\langle e\left|\frac{\partial H}{\partial q_k}\right|e\right\rangle\right]_0 \langle u|q_k|v\rangle, \tag{13}$$

$$B'_{ij} = -\frac{2}{\hbar^2}\sum_e \sum_{s>e} \frac{(\omega_e\omega_s+\omega_0^2)}{(\omega_e^2-\omega_0^2)(\omega_s^2-\omega_0^2)}[(M_i)^0_{ge}(M_j)^0_{gs} + (M_j)^0_{ge}(M_i)^0_{gs}]\sum_k \left[\left\langle e\left|\frac{\partial H}{\partial q_k}\right|s\right\rangle\right]_0 \langle u|q_k|v\rangle, \tag{14}$$

where the C term is incorporated into the B' term, and these are the Franck–Condon term (the A term) and the vibronic-coupling term (the B term).

In the present paper the following approximations are employed. First, only the in-plane modes are considered, which play a dominant role for the $\pi-\pi^*$ transitions, and are obtained based on the semi-empirical force constants.[79] Second, the Pariser–Parr–Pople approximation[76,77] is employed for SCF CI calculations combined with the Nishimoto–Mataga approximation for the electron repulsion integrals.[78] Here we recall that the perturbation expansion of the electronic wave function is related with those for the configuration interaction expansion. The first-order perturbation theory gives the wave function

$$|\Psi_e(\boldsymbol{q})\rangle = \sum_s \sum_k c_{es}(q_k)|\Psi_s(0)\rangle, \tag{15}$$

where

$$c_{es}(q_k) = \frac{\left[\left\langle e\left|\frac{\partial H}{\partial q_k}\right|s\right\rangle\right]_0 q_k}{E^0_e - E^0_s}, \quad \text{for } s\neq e, \tag{16}$$

$$c_{ee}(q_k) = 1. \tag{17}$$

On the other hand the CI expansion at $\boldsymbol{q}$ is

$$|\Psi_i(\boldsymbol{q})\rangle = \sum_t a_{it}(\boldsymbol{q})|\Phi_t(\boldsymbol{q})\rangle. \tag{18}$$

Substituting Eq. (15) with Eq. (18) yields

$$\sum_t a_{et}(\boldsymbol{q})|\Phi_t(\boldsymbol{q})\rangle = \sum_s \sum_k c_{es}(q_k)|\Psi_s(0)\rangle, \tag{19}$$

and multiplying the complex conjugate of

$$|\Psi_s(0)\rangle = \sum_{t'} a_{st'}(0)|\Phi_{t'}(0)\rangle, \tag{20}$$

on both sides, and integrating on the assumption of

$$\langle\Phi_{t'}(0)|\Phi_t(\boldsymbol{q})\rangle = \delta_{t't}, \tag{21}$$

leads to

$$\sum_t a^*_{st}(0)a_{et}(\boldsymbol{q}) = \sum_k c_{es}(q_k). \tag{22}$$

Therefore, the perturbation coefficients $c_{es}(q_k)$ are obtained from the CI coefficients a_{et}. The derivative of the transition moment with respect to q_k [Eq. (9)] is deduced from the CI expansion coefficients according to Eq. (22). Third, only one component, $|\alpha_{ii}|^2$, of the polarizability tensor is taken into account without the isotropic averaging of the molecular orientation.[123]

VI. CONCLUSIONS

The vibrational spectra of the [*n*]oligoacenes ($n=2-5$) are understood systematically in conjunction with the dispersion relations of polyacene. The diradical states do not give rise to dramatic features for vibrational frequencies and infrared intensities. Observation of the resonance Raman effect for the 1064-nm excitation is somewhat surprising, since for pyrene the nonresonant Raman calculations for the 514.5-nm excitation (2.41 eV) agree with experiment.[44] Polyacene presents surprisingly good relevance to the real systems including graphite and polyacetylene. The present combined approach with the *ab initio* density functional calculations and the predictive excited states vibronic calculations can be extended to larger systems such as polyacene ribbons and carbon nanotubes.[65] The dispersion relations reported by Dresselhaus and co-workers have described the essential properties of carbon nanotubes,[24,30,62] however, higher effects including those from double walls and H-atom capping could be reached using the present approach. The zone folding method demonstrated here would be of use for understanding of the intermediate region of nanosize materials or clusters.

ACKNOWLEDGMENTS

This work was supported by a 21st century COE program from the Ministry of Education, Science, Sports, and Culture of Japan, by a Grant-in-Aids for Scientific Research (C) from the Japan Society for the Promotion of Science, and by a Research Grant from the Matsuo Foundation.

[1] *Spectral Atlas of Polycyclic Aromatic Compounds, Including Data on Occurrence and Biological Activity*, edited by W. Karcher, R. J. Fordham, J. J. Dubois, P. G. J. M. Glaude, and J. A. M. Ligthart (Kluwer, Hingham, MA, 1985), Vols. 1 and 2.
[2] *Polycyclic Aromatic Hydrocarbons and Astrophysics*, NATO ASI Series, edited by A. Léger, L. d'Hendecourt, and N. Boccara (Reidel, Holland, 1987).
[3] R. G. Harvey, *Polycyclic Aromatic Hydrocarbons* (Wiley-VCH, New York, 1997).
[4] J. L. Puget and A. Léger, Annu. Rev. Astron. Astrophys. **27**, 161 (1989).
[5] S. R. Langhoff, J. Phys. Chem. **100**, 2819 (1996).
[6] D. M. Hudgins and S. A. Sandford, J. Phys. Chem. A **102**, 329 (1998).
[7] E. Clar, *Polycyclic Hydrocarbons* (Academic, London, 1964).
[8] J. B. Birks, *Photophysics of Aromatic Molecules* (Wiley, London, 1970).
[9] *Single-Molecule Optical Detection, Imaging and Spectroscopy*, edited by T. Basché, W. E. Moerner, M. Orrit, and U. P. Wild (VCH, Weinheim, 1997).
[10] *The Fullerenes*, edited by H. W. Kroto, J. E. Fischer, and D. E. Cox (Pergamon, Oxford, 1993).
[11] M. Endo, S. Iijima, and M. S. Dresselhaus, *Carbon Nanotubes* (Pergamon, Oxford, 1996).
[12] J. R. Sheats, J. Mater. Res. **19**, 1974 (2004).
[13] G. Horowitz, Adv. Mater. **10**, 365 (1998).
[14] C. D. Dimitrakopoulos and P. R. L. Malenfant, Adv. Mater. **14**, 99 (2002).
[15] S. F. Nelson, Y.-Y. Lin, D. J. Gundlach, and T. N. Jackson, Appl. Phys. Lett. **72**, 1854 (1998).
[16] J. Cornil, J. Ph. Calbert, and J. L. Brédas, J. Am. Chem. Soc. **123**, 1250 (2001).
[17] V. Y. Butko, X. Chi, D. V. Lang, and A. P. Ramirez, Appl. Phys. Lett. **83**, 4773 (2003).
[18] M. M. Payne, S. R. Parkin, J. E. Anthony, C.-C. Kuo, and T. N. Jackson, J. Am. Chem. Soc. **127**, 4986 (2005).
[19] F.-J. Meyer zu Heringdorf, M. C. Reuter, and R. M. Tromp, Nature (London) **412**, 517 (2001).
[20] M. Cazayous, A. Sacuto, G. Horowitz, Ph. Lang, A. Zimmers, and R. P. S. M. Lobo, Phys. Rev. B **70**, 081309 (2004).
[21] R. He, I. Dujovne, L. Chen, Q. Miao, C. F. Hirjibehedin, A. Pinczuk, C. Nuckolls, C. Kloc, and A. Ron, Appl. Phys. Lett. **84**, 987 (2004).
[22] C. B. France, P. G. Schroeder, J. C. Forsythe, and B. A. Parkinson, Langmuir **19**, 1274 (2003).
[23] Q. Chen, A. J. McDowall, and N. V. Richardson, Langmuir **19**, 10164 (2003).
[24] *Physical Properties of Carbon Nanotubes*, edited by R. Saito, G. Dresselhaus, and M. S. Dresselhaus (Imperial College Press, London, 1998).
[25] M. Bockrath, D. H. Cobden, P. L. McEuen, N. G. Chopra, A. Zettl, A. Thess, and R. E. Smalley, Science **275**, 1922 (1997).
[26] P. Jarillo-Herrero, J. A. van Dam, and L. P. Kouwenhoven, Nature (London) **439**, 953 (2006).
[27] V. R. Coluci, D. S. Galvão, and A. Joro, Nanotechnology **17**, 617 (2006).
[28] A. C. Dillon, P. A. Parilla, J. L. Alleman, T. Gennett, K. M. Jones, and M. J. Heben, Chem. Phys. Lett. **401**, 522 (2005).
[29] L. C. Venema, J. W. G. Wildöer, H. L. J. T. Tuinstra, C. Dekker, A. G. Rinzler, and R. E. Smalley, Appl. Phys. Lett. **71**, 2629 (1997).
[30] A. M. Rao, E. Richter, S. Bandow *et al.*, Science **275**, 187 (1997).
[31] E. Heilbronner and J. P. Maier, in *Electron Spectroscopy: Theory, Techniques and Applications*, edited by C. R. Brundle and A. D. Baker (Academic, London, 1977), Vol. 1, Chap. 5.
[32] Y. Kim, T. Komeda, and M. Kawai, Phys. Rev. Lett. **89**, 126104 (2002).
[33] T. A. Yano, Y. Inouye, and S. Kawata, Nano Lett. **6**, 1269 (2006).
[34] R. P. Vidano, D. B. Fischbach, L. J. Williams, and T. M. Loeher, Solid State Commun. **39**, 341 (1981).
[35] J. Kastner, T. Pichler, H. Kuzmany, S. Curran, W. Blau, D. N. Weldon, M. Delamesiere, S. Draper, and H. Zandbergen, Chem. Phys. Lett. **221**, 53 (1994).
[36] W. Zhou, M. F. Islam, H. Wang, D. L. Ho, A. G. Yodh, K. I. Winey, and J. E. Fischer, Chem. Phys. Lett. **384**, 185 (2004).
[37] J. Maultzsch, S. Reich, C. Thomsen, H. Requardt, and P. Ordejón, Phys. Rev. Lett. **92**, 075501 (2004).
[38] T. Aizawa, R. Souda, S. Otani, Y. Ishizawa, and C. Oshima, Phys. Rev. B **42**, 11469 (1990).
[39] C. Oshima, T. Aizawa, R. Souda, and Y. Sumimyoshi, Solid State Commun. **65**, 1601 (1988).
[40] For example, *Molecular Dynamics and Spectroscopy by Stimulated Emission Pumping*, edited by D. Hai-Lung and R. W. Field (World Scientific, Singapore, 1995).
[41] H. H. Heinze, A. Görling, and N. Rösch, J. Chem. Phys. **113**, 2088 (2000).
[42] M. S. Deleuze, L. Claes, E. S. Kryachko, and J.-P. François, J. Chem. Phys. **119**, 3106 (2003).
[43] S. Hirata, M. Head-Gordon, J. Szczepanski, and M. Vala, J. Phys. Chem. A **107**, 4940 (2003).
[44] L. Jensen, L. L. Zhao, J. Autschbach, and G. C. Schatz, J. Chem. Phys. **123**, 174110 (2005).
[45] R. A. Hites and W. J. Simonsick, Jr., *Calculated Molecular Properties of Polycyclic Aromatic Hydrocarbons*, Physical Sciences Data 29 (Elsevier, Amsterdam, 1987).

[46] B. Pullman, Int. J. Quantum Chem. **16**, 669 (1979).
[47] K. Ohno, J. Mol. Spectrosc. **72**, 238 (1978).
[48] K. Ohno, J. Mol. Spectrosc. **77**, 329 (1979).
[49] C. A. Coulson and H. C. Longuet-Higgins, Proc. R. Soc. London, Ser. A **A193**, 456 (1948).
[50] M. Bendikov, H. M. Duong, K. Starkey, K. N. Houk, E. A. Carter, and F. Wudl, J. Am. Chem. Soc. **126**, 7416 (2004).
[51] W. J. Bailey and C. Liao, J. Am. Chem. Soc. **77**, 992 (1955).
[52] M. M. Payne, S. R. Parkin, and J. E. Anthony, J. Am. Chem. Soc. **127**, 8028 (2005).
[53] J. Aihara, J. Chem. Soc., Perkin Trans. 2 **1994**, 971 (1994).
[54] K. N. Houk, P. S. Lee, and M. Nendel, J. Org. Chem. **66**, 5517 (2001).
[55] J.-M. André, B. Champagne, E. A. Perpéte, and M. Guillaume, Int. J. Quantum Chem. **84**, 607 (2001).
[56] J. Poater, J. M. Bofill, P. Alemany, and M. Solà, J. Phys. Chem. A **109**, 10629 (2005).
[57] A. Hinchliffe, A. Nikolaidi, S. Machado, and J. Humberto, Cent. Eur. J. Chem. **3**, 361 (2005).
[58] Y. Yamakita and K. Ohno, The Symposium on Molecular Structure, Nagoya, 1997, 3PA70; J. Kimura, Y. Yamakita, and K. Ohno, The Annual Meeting of the Chemical Society of Japan, Kyoto, 1998, 2PB011.
[59] C. Castiglioni, C. Mapelli, F. Negri, and G. Zerbi, J. Chem. Phys. **114**, 963 (2001).
[60] C. Mapelli, C. Castiglioni, and G. Zerbi, Phys. Rev. B **60**, 12710 (1999).
[61] C. Thomsen and S. Reich, Phys. Rev. Lett. **85**, 5214 (2000).
[62] R. A. Jishi, L. Venkataraman, M. S. Dresselhaus, and G. Dresselhaus, Chem. Phys. Lett. **209**, 77 (1993).
[63] T. Yumura, D. Nozaki, S. Bandow, K. Yoshizawa, and S. Iijima, J. Am. Chem. Soc. **127**, 11769 (2005).
[64] K. Nakada, M. Fujita, G. Dresselhaus, and M. S. Dresselhaus, Phys. Rev. B **54**, 17954 (1996).
[65] M. Yamada, Y. Yamakita, and K. Ohno (unpublished).
[66] H. Shinohara, Y. Yamakita, and K. Ohno, J. Mol. Struct. **442**, 221 (1998).
[67] M. J. Frisch, G. W. Trucks, H. B. Schlegel *et al.*, Gaussian 03, Revision D.01; Gaussian, Inc., Wallingford CT, 2004.
[68] A. D. Becke, J. Chem. Phys. **98**, 5648 (1993).
[69] C. Lee, W. Yang, and R. G. Parr, Phys. Rev. B **37**, 785 (1988).
[70] Y. Yamakita, Y. Isogai, and K. Ohno, J. Chem. Phys. **124**, 104301 (2006).
[71] G. Placzek, in *Handbuch der Radiologie,* edited by E. Marx (Akademische Verlag, Leipzig, 1934), Vol. 6, Part 2, p. 205.
[72] D. A. Long, *Raman Spectroscopy* (MacGraw-Hill, New York, 1977).
[73] H. A. Kramers and W. Heisenberg, Z. Phys. **31**, 681 (1925).
[74] P. A. M. Dirac, Proc. R. Soc. London, Ser. A **A114**, 710 (1927).
[75] A. C. Albrecht, J. Chem. Phys. **34**, 1476 (1961).
[76] R. Pariser and R. G. Parr, J. Chem. Phys. **21**, 446 (1953).
[77] J. A. Pople, Trans. Faraday Soc. **49**, 1375 (1953).
[78] K. Nishimoto and N. Mataga, Z. Phys. Chem. **12**, 335 (1957).
[79] K. Ohno, J. Chem. Phys. **95**, 5524 (1991), and references therein.
[80] S. N. Ketkar and M. Fink, J. Mol. Struct. **77**, 139 (1981).
[81] C. P. Brock, J. D. Dunitz, and F. L. Hirshfeld, Acta Crystallogr., Sect. B: Struct. Sci. **47**, 789 (1991).
[82] S. N. Ketker, M. Kelley, M. Fink, and R. C. Ivey, J. Mol. Struct. **77**, 127 (1981).
[83] R. B. Campbell and J. M. Robertson, Acta Crystallogr. **15**, 289 (1962).
[84] E. S. Kadantsev, M. J. Stott, and A. Rubio, J. Chem. Phys. **124**, 134901 (2006).
[85] D. E. Freeman and I. G. Ross, Spectrochim. Acta, Part A **16**, 1393 (1960).
[86] D. B. Scully and D. H. Whiffen, Spectrochim. Acta, Part A **16**, 1409 (1960).
[87] J. R. Scherer, J. Chem. Phys. **36**, 3308 (1962).
[88] N. Neto, M. Scrocco, and S. Califano, Spectrochim. Acta, Part A **22**, 1981 (1966).
[89] D. M. Hanson and A. R. Gee, J. Chem. Phys. **51**, 5052 (1969).
[90] A. Bakke, V. N. Cyvin, J. C. Whiter, S. J. Cyvin, J. E. Gustavsen, and P. Klaeboe, Z. Naturforsch. A **34A**, 579 (1979).
[91] G. Neerland, B. N. Cyvin, J. Brunvoll, S. J. Cyvin, and P. Klaeboe, Z. Naturforsch. A **35A**, 1390 (1980).
[92] H. Sellers, P. Pulay, and J. E. Boggs, J. Am. Chem. Soc. **107**, 6487 (1985).
[93] F. Negri and M. Zgierski, J. Chem. Phys. **104**, 3486 (1996).
[94] J. Szczepanski, M. Valla, D. Talbi, O. Parisel, and Y. Ellinger, J. Chem. Phys. **98**, 4494 (1993).
[95] S. Zilberg, Y. Haas, and S. Shaik, J. Phys. Chem. **99**, 16558 (1995).
[96] D. Chakarborty, R. Ambashta, and S. Manogaran, J. Phys. Chem. **100**, 13963 (1996).
[97] J. M. L. Martin, J. El-Yazal, and J.-P. François, J. Phys. Chem. **100**, 15358 (1996).
[98] S. S. Mitra and H. J. Bernstein, Can. J. Chem. **37**, 553 (1959).
[99] N. A. Abasbegović, N. Vukotić, and L. Colombo, J. Chem. Phys. **41**, 2575 (1964).
[100] M. Suzuki, T. Yokoyama, and M. Ito, Spectrochim. Acta, Part A **24**, 1091 (1968).
[101] F. Stenman, J. Chem. Phys. **54**, 4217 (1971).
[102] N. J. Bridge and D. Vincent, J. Chem. Soc., Faraday Trans. 2 **68**, 1522 (1972).
[103] J. Räsänen, F. Stenman, and E. Penttnen, Spectrochim. Acta, Part A **29**, 395 (1973).
[104] W. F. Maddams and A. M. Royaud, Spectrochim. Acta, Part A **46**, 309 (1990).
[105] M. Rumi, G. Zerbi, K. Müllen, G. Müller, and M. Rehahn, J. Chem. Phys. **106**, 24 (1997).
[106] N. Ohta and M. Ito, J. Chem. Phys. **65**, 2907 (1976).
[107] N. Ohta and M. Ito, Chem. Phys. **20**, 71 (1977).
[108] G. R. Loppnow, L. Shoute, K. J. Schmidt, A. Savage, R. H. Hall, and J. T. Bulmer Philos. Trans. R. Soc. London, Ser. A **362**, 2461 (2004).
[109] E. V. Efremov, F. Ariese, A. J. G. Mank, and C. Gooijer, Anal. Chem. **78**, 3152 (2006).
[110] J. M. Hollas, J. Mol. Spectrosc. **9**, 138 (1962).
[111] D. M. Hanson, J. Chem. Phys. **51**, 5063 (1969).
[112] F. M. Behlen, D. B. McDonald, V. Sethuraman, and S. A. Rice, J. Chem. Phys. **75**, 5685 (1981).
[113] A. Amirav, U. Even, and J. Jortner, J. Chem. Phys. **75**, 3770 (1981).
[114] D. M. Hudgins and S. A. Sandford, J. Phys. Chem. A **102**, 344 (1998).
[115] G. Filippini and C. M. Gramaccioli, Chem. Phys. Lett. **104**, 50 (1984).
[116] A. Brillante, R. G. D. Valle, L. Farina, A. Girlando, M. Masino, and E. Venuti, Chem. Phys. Lett. **357**, 32 (2002).
[117] E. Venuti, R. G. D. Valle, A. Brillante, M. Masino, and A. Girlando, J. Am. Chem. Soc. **124**, 2128 (2002).
[118] R. G. Della Valle, E. Venuti, L. Farina, A. Brillante, M. Masino, and A. Girlando, J. Phys. Chem. B **108**, 1822 (2004).
[119] E. L. Bokhenkov, A. I. Kolesnikov, T. A. Krivenko, E. F. Sheka, and V. A. Dementjev, J. Phys. C **6**, 566 (1981).
[120] D. Biermann and W. Schmidt, J. Am. Chem. Soc. **102**, 3163 (1980).
[121] J. Neugebauer, E. J. Baerends, E. V. Efremov, F. Ariese, and C. Gooijer, J. Phys. Chem. A **109**, 2100 (2005), and references therein.
[122] S. Matsunuma, N. Akamatsu, T. Kamisuki, Y. Adachi, S. Maeda, and C. Hirose, J. Chem. Phys. **88**, 2956 (1988).
[123] A. C. Albrecht and M. C. Hutley, J. Chem. Phys. **55**, 4438 (1971).
[124] J. Tang and A. C. Albrecht, in *Raman Spectroscopy*, edited by H. A. Szymanski (Plenum, New York, 1970), Vol. 2, Chap. 2.
[125] For example, L. D. Landau and E. M. Lifshitz, *Theory of Elasticity*, 3rd ed. (Pergamon, Oxford, 1986).
[126] M. J. Matthews, M. A. Pimenta, G. Dresselhaus, M. S. Dresselhaus, and M. Endo, Phys. Rev. B **59**, R6585 (1999).
[127] J. Maultzsch, S. Reich, and C. Thomsen, Phys. Rev. B **64**, 121407 (2001).
[128] S. Hirata and M. Tasumi, J. Chem. Phys. **103**, 8964 (1995).
[129] G. L. Squires, *Introduction to the Theory of Neutron Scattering* (Dover, New York, 1978).